Volume 1 | Number 1 | Jan 2013 | Pages 1–100

Chemical Science

www.rsc.org/chemicalscience

ROYAL SOCIETY OF CHEMISTRY

ROYAL SOCIETY OF CHEMISTRY

www.rsc.org/chemicalscience

Journal Name

ARTICLE

Protonation state of the Cu_4S_2 Cu_Z site in nitrous oxide reductase: redox dependence and insight into reactivity

Esther M. Johnston,[a] Simone Dell'Acqua[b], Sofia R. Pauleta[c], Isabel Moura[c] and Edward I. Solomon[a*]

Spectroscopic and computational methods have been used to determine the protonation state of the edge sulfur ligand in the Cu_4S_2 Cu_Z form of the active site of nitrous oxide reductase (N_2OR) in its $3Cu^ICu^{II}$ (1-hole) and $2Cu^I2Cu^{II}$ (2-hole) redox states. The EPR, absorption, and MCD spectra of 1-hole Cu_Z indicate that the unpaired spin in this site is evenly delocalized over Cu_I, Cu_{II}, and Cu_{IV}. 1-hole Cu_Z is shown to have a μ_2-thiolate edge ligand from the observation of S-H bending modes in the resonance Raman spectrum at 450 and 492 cm^{-1} that have significant deuterium isotope shifts (-137 cm^{-1}) and are not perturbed up to pH 10. 2-hole Cu_Z is characterized with absorption and resonance Raman spectroscopies as having two Cu-S stretching vibrations that profile differently. DFT models of the 1-hole and 2-hole Cu_Z sites are correlated to these spectroscopic features to determine that 2-hole Cu_Z has a μ_2-sulfide edge ligand at neutral pH. The slow two electron (+1 proton) reduction of N_2O by 1-hole Cu_Z is discussed and the possibility of a reaction between 2-hole Cu_Z and O_2 is considered.

1. Introduction

The main reductive part of the nitrogen cycle, known as bacterial denitrification, is performed by soil and marine bacteria as a means of anaerobic or microaerobic respiration. Denitrification involves the conversion of nitrate to dinitrogen via four successive reductive steps ($NO_3^- \rightarrow NO_2^- \rightarrow NO \rightarrow N_2O \rightarrow N_2$), each performed by a different metalloenzyme.[1] The terminal product of denitrification can be either N_2O or N_2, depending on the regulatory control of the N_2O reduction process and whether the bacterium involved contains the gene cluster for nitrous oxide reduction (the *nos* cluster; *nosZ* encodes the nitrous oxide reductase enzyme).[2, 3] The N_2O reduction process and its regulation *in vivo* are of significant interest because N_2O is a potent greenhouse gas, with a global warming potential 300x that of CO_2,[4, 5] and depletes the ozone layer.[6] Anthropogenic sources of environmental N_2O, the majority of which is due to agricultural activity, is an increasing contribution to the global atmosphere.[2] Soil studies have indicated that pH,[7, 8] temperature,[9] acetylene,[10] sulfide,[11] and dioxygen[12] all affect the production of N_2O, but the molecular basis of these effects is still not known. A molecular understanding of nitrous oxide reduction and how this process is regulated could enable mitigation of N_2O release from anthropogenic sources.[5]

Nitrous oxide reductase contains two copper sites: a binuclear site known as Cu_A that functions as an electron transfer site, and an unusual tetranuclear copper sulfide cluster active site, where N_2O binds and is reduced (Figure 1). Two forms of this tetranuclear site have been structurally characterized. One, known as Cu_Z^*, has a μ_4 sulfide ligand bridging all four coppers and a solvent derived ligand on an open edge (the Cu_I-Cu_{IV} edge) where N_2O is proposed to bind (Figure 1A).[13] This edge ligand has previously been assigned as
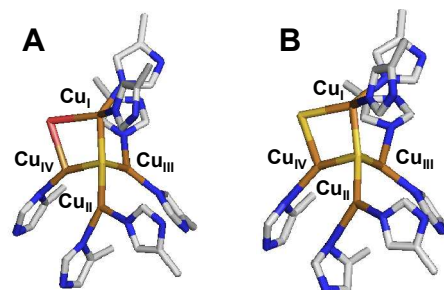
Figure 1: The two forms of the tetranuclear copper sulfide active site of nitrous oxide reductase. A) Cu_Z^* in PdN$_2$OR isolated aerobically (PDB ID 1FWX).[13] B) Cu_Z in PsN$_2$OR isolated anaerobically (PDB ID 3SBP).[14]

a bridging hydroxide ligand, due to the presence of a vibration in the resonance Raman spectrum of Cu_Z^* that shifts in $H_2^{18}O$ solvent at high pH and the absence of significant spectroscopic

differences between Cu$_Z$* at high and low pH.[15] The other form of the cluster, known as Cu$_Z$, has an additional μ$_2$ sulfur ligand bridging the Cu$_I$-Cu$_{IV}$ edge (Figure 1B).[14] Whether the μ$_2$ edge ligand in Cu$_Z$ is a thiolate (SH$^-$) or a sulfide (S^{2-}) and how its protonation depends on the redox state of the cluster are not known. The Cu$_4$S$_2$ Cu$_Z$ form of the cluster is dominantly isolated when N$_2$OR is purified in the absence of oxygen[16] or rapidly in the presence of oxygen,[17] while the Cu$_4$S Cu$_Z$* form is isolated when the purification is performed aerobically or anaerobically from mutants in the accessory genes;[16-18] however, all purifications typically yield enzyme with a mixture of the two sites.[17, 19] Which structural form of the cluster is responsible for N$_2$O reduction *in vivo* is a matter of some debate.[20-22] As isolated, neither N$_2$OR containing a high percentage of Cu$_Z$ nor N$_2$OR containing a high percentage of Cu$_Z$* shows high enough specific activity in steady-state assays to be consistent with N$_2$OR activity in whole cells.[17, 23] N$_2$OR containing Cu$_Z$ can be activated by prolonged dialysis against base,[23] while N$_2$OR that contains Cu$_Z$* can be reductively activated by preincubation with methyl viologen, which reduces Cu$_Z$* to the active fully reduced (4Cu^I) redox state.[24, 25] After activation, both Cu$_Z$ and Cu$_Z$* show specific activities consistent with whole cell N$_2$OR activity.[20, 23] However, it has recently been shown that the Cu$_Z$* site in its fully reduced redox state is the form of the cluster that is responsible for the rapid N$_2$O reduction in steady state assays with methyl viologen, based on its rapid single turnover reaction with N$_2$O. Alternatively, in single turnover studies Cu$_Z$ in its 1-hole redox state reduces N$_2$O but at a rate too slow to be catalytically relevant (10^{-6} that of the fully reduced state of Cu$_Z$*).[26] Thus, the physiological role of the Cu$_Z$ site in nitrous oxide reduction and whether it participates in N$_2$O reduction *in vivo* are unknown.

The Cu$_Z$ site in nitrous oxide reductase has been extensively studied in N$_2$OR isolated from *Pseudomonas stutzeri* (*Ps*N$_2$OR)[27, 28] and *Paracoccus pantotrophus* (*Pp*N$_2$OR).[19, 29] In the latter enzyme, Cu$_Z$ has been shown to access two redox states, the resting 2Cu^{I}2Cu^{II} (2-hole) redox state, and a 1 electron reduced 3Cu^{I}Cu^{II} (1-hole) redox state (E^o = +60 mV).[19] Both redox states of Cu$_Z$ have previously been studied using EPR, absorption, MCD, and resonance Raman spectroscopies.[19, 28, 30-33] However, these studies were performed before the elucidation of the presence of a second sulfur in the Cu$_Z$ cluster, and so yielded limited direct insight into the cluster and the protonation state of the edge sulfur. Additionally, the previous studies were performed in the presence of background spectroscopic features from ~30% Cu$_Z$*, which complicates the analysis.[19, 29] These limitations lead to the conclusion that Cu$_Z$ and Cu$_Z$* were very similar and perhaps differed only in the second sphere.[28] These results are now extended and correlated to the structural insight that Cu$_Z$ contains an additional inorganic sulfur edge ligand.[14] An understanding of the protonation state, electronic structure, and potential reactivity of the Cu$_Z$ site is necessary to gain insight into its reactivity and role *in vivo*.

This study uses EPR, absorption, MCD and resonance Raman spectroscopies coupled with DFT calculations to determine the protonation state of the edge sulfur ligand in the 1-hole and 2-hole redox states of Cu$_Z$ in *Marinobacter hydrocarbonoclasticus* N$_2$OR (*Mh*N$_2$OR) and to define the electronic structures of these states. This leads to insight into the nature of the reactivity of the 1-hole and 2-hole states of Cu$_Z$ and the origin of the spectroscopic similarity between 1-hole Cu$_Z$ and 1-hole Cu$_Z$*, despite significant differences in edge ligation in the two sites.

2. Methodology

2.1 Summary of Experimental Methodology

Full experimental methodology and computational details can be found in the Electronic Supporting Information, while a summary is presented here. Nitrous oxide reductase (N$_2$OR) was isolated from *Marinobacter hydrocarbonoclasticus* 617 (formerly *Pseudomonas nautica*) grown under microaerobic conditions in the presence of nitrate after two aerobic chromatographic steps without added reductant, as described previously.[17] These purification conditions were shown to maximize the amount of Cu$_4$S$_2$ Cu$_Z$ content relative to Cu$_4$S Cu$_Z$* in the purified enzyme. Samples containing larger amounts of Cu$_Z$* were purified in parallel with three chromatographic purification steps from a batch of cells grown under anaerobic conditions in the presence of nitrate, and that had been stored at -80 ºC for a long period.[17, 26] Both MhN$_2$OR showed copper quantitation results consistent with fully occupancy of the Cu$_A$ and Cu$_Z$/Cu$_Z$* sites (6.4±0.2 and 6.2±0.7 respectively). The percentage of Cu$_Z$ versus Cu$_Z$* in the samples used for this study was determined by EPR spin quantitation (Figure S1). Samples purified with high amounts of Cu$_Z$ contained 60±10% Cu$_Z$, while samples purified to obtain more Cu$_Z$* contained 10±10% Cu$_Z$. Spectroscopic samples of 1-hole and 2-hole Cu$_Z$ were prepared in a glove box under N$_2$ atmosphere. Samples of 1-hole Cu$_Z$ were prepared from *Mh*N$_2$OR (60% Cu$_Z$ and 40% Cu$_Z$*) that had been incubated with 100 equivalents of reduced methyl viologen, with subsequent removal of the methyl viologen using a desalting column. Samples of 2-hole Cu$_Z$ were prepared by reducing *Mh*N$_2$OR (60±10% Cu$_Z$, 40±10% Cu$_Z$*) with 10 equivalents of sodium ascorbate, which reduces the Cu$_A$ site rapidly and the 2-hole Cu$_Z$ site very slowly, and spectra were collected within 1 hour so that minimal reduction of 2-hole Cu$_Z$ was observed. In parallel, MhN$_2$OR samples containing 90±10% Cu$_Z$* were reduced with 10 equivalents of sodium ascorbate to obtain the spectral features of 1-hole Cu$_Z$*. For pH and deuteration studies, samples of 1-hole and 2-hole Cu$_Z$ were buffer exchanged by centrifugation into different pH or pD buffers. Typical *Mh*N$_2$OR concentrations used for spectroscopic samples were 0.1-0.3 mM for absorption, MCD and EPR, and up to 0.5 mM for resonance Raman.

2.2 Computational Modeling

A computational model of Cu_Z was built from the atomic coordinates of the crystal structure of *Pseudomonas stutzeri* N_2OR, the only known structure of the Cu_4S_2 cluster (PDB ID 3SBP, resolution 1.7 Å).[14] The model included the Cu_4S_2 core and 7 ligating His residues, where the α carbon and distal nitrogen were constrained at their crystallographic positions. A computational model for Cu_Z* with a hydroxide bridging ligand and identical α carbon and distal nitrogen constraints was constructed from the crystal structure of *Paracoccus denitrificans* N_2OR (*Pd*N_2OR, PDB ID 1FWX).[13] Calculations were performed using Gaussian 09 (version d01).[34] Geometry optimizations were performed using the B3LYP functional, the TZVP basis set on all core atoms (Cu_4S) and the ligating His nitrogens, and the SV basis set on all remaining atoms, and solvation was modeled with a PCM of 4.0. A larger basis set and different functionals were also explored, as described in the text. The optimized structures were then used for frequency, TD DFT, and single point calculations. To determine the relative energy of deprotonation (ΔΔE) of the edge SH^- in the 2-hole versus 1-hole redox state, larger models were optimized that included two second sphere carboxylates, Asp127 and Asp240, which hydrogen bond to the His ligands of Cu_I and Cu_{II}. The energy of an internal proton transfer from the edge SH^- to Asp127 was calculated for the 1-hole and 2-hole redox states and compared to obtain the ΔΔE.

3 Results and Analysis

3.1 Spectroscopy of 1-hole Cu_Z

Previous spectroscopic studies of Cu_Z, undertaken before identification of the presence of a second sulfur, were performed on samples of *Pp*N_2OR and *Ps*N_2OR that contained mixtures of the Cu_Z and Cu_Z* sites (in a 7:3 ratio for *Pp*N_2OR) without a way to resolve the spectral features of the Cu_Z site from the mixture.[19, 28, 29] Recently, it has been found that the two-sulfur Cu_Z site cannot be reduced by methyl viologen, which reduces both the Cu_A site and the Cu_Z* form of the cluster.[26] This provides an opportunity to cleanly resolve the spectral features of 1-hole Cu_Z by studying methyl viologen reduced samples after removal of the reductant. This approach allows correlation of the electronic structure of 1-hole Cu_Z, obtained from spectroscopy, with the recently determined Cu_4S_2 structure of the cluster, to determine the nature of the edge sulfur ligand in its 1-hole and resting 2-hole redox states. **EPR** The X-band and Q-band EPR spectra of a methyl viologen reduced sample of 1-hole Cu_Z are given in Figure 2. The EPR spectrum is axial with $g_\parallel > g_\perp > 2.0$ and a pattern of five evenly space hyperfine lines in the $A_\parallel$ region. The axial nature of the spectrum indicates that, while the spin density is delocalized over multiple copper nuclei, it resides in dominantly d_{x2-y2} orbitals on each Cu site that contributes to the ground state. The $A_\parallel$ hyperfine features can be further resolved in the second derivative of the X-band EPR spectrum, as can hyperfine features in the $A_\perp$ region (Figure 2A inset and Figure S2).Simulation of the X-band, X-band 2nd derivative, and Q-
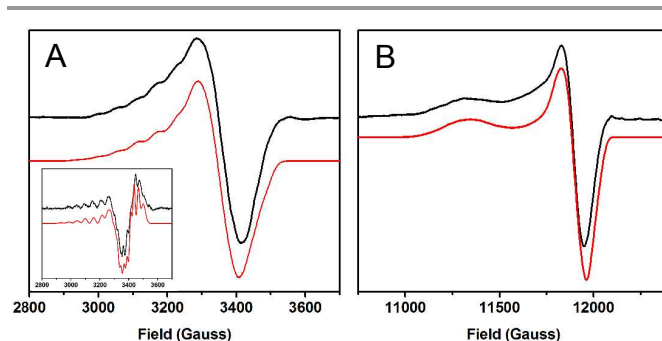

Figure 2: EPR spectra of 1-hole Cu_Z (black) with simulations (red). A) X-band at 77 K, 9.6349 GHz. Inset: 2nd derivative of the X-band. B) Q-band at 77 K, 34.082 GHz.

band EPR spectra yields the g and A values for 1-hole Cu_Z given in Table 1. The g values for 1-hole Cu_Z are very similar

Table 1: EPR g and A values for 1-hole Cu_Z, obtained from simulations included in Figure 2 and Figure S2 with values for Cu_Z* reproduced from Reference [15].

	1-hole Cu_Z	1-hole Cu_Z*
$g_\parallel$	2.152	2.160
$A_\parallel$	$56\times10^{-4}\,cm^{-1}$	$61\times10^{-4}\,cm^{-1}$
	$56\times10^{-4}\,cm^{-1}$	$23\times10^{-4}\,cm^{-1}$
	$56\times10^{-4}\,cm^{-1}$	
$g_\perp$	2.042	2.043
$A_\perp$	$20\times10^{-4}\,cm^{-1}$	$25\times10^{-4}\,cm^{-1}$
	$20\times10^{-4}\,cm^{-1}$	$20\times10^{-4}\,cm^{-1}$
	$20\times10^{-4}\,cm^{-1}$	

to those previously obtained for 1-hole Cu_Z* (Table 1) and to those obtained for Cu_Z in *Pp*N_2OR.[15, 29] This is interesting, considering that an edge SH^- (thiolate) or S^{2-} (sulfide) in Cu_Z would be expected to be a more covalent ligand than the hydroxide in Cu_Z*[15] and this would lower the g values. However, in 1-hole Cu_Z* there is a high energy d-d transition that is not present in the 1-hole Cu_Z spectrum (vide infra). This transition has previously been assigned as a $d_{xy} \rightarrow d_{x2-y2}$ excitation localized on Cu_I.[35] The $g_\parallel$ value is inversely proportional to the d_{xy} to d_{x2-y2} energy splitting, so the presence of a high energy $d_{xy} \rightarrow d_{x2-y2}$ transition in Cu_Z* but not in Cu_Z would lead to a lower $g_\parallel$ value for Cu_Z* than would be expected from covalency alone, which could result in similar $g_\parallel$ values between 1-hole Cu_Z* and the more covalent 1-hole Cu_Z site. The ligand field origin of the lower energy $d_{xy} \rightarrow d_{x2-y2}$ transition in 1-hole Cu_Z is considered below.

The $A_\parallel$ and $A_\perp$ values for 1-hole Cu_Z are similar in magnitude to those for Cu_Z*, but fitting the hyperfine pattern requires three equivalent contributions rather than the ~5:2 ratio of hyperfine values observed for Cu_Z* (Table 1).[36] This indicates that in the ground state of 1-hole Cu_Z the spin is distributed over three copper centers in dominantly d_{x2-y2} orbitals. The three coppers involved are likely Cu_I, Cu_{II}, and Cu_{IV}, since these copper centers are in the same plane as the two sulfur ligands and bonding with the strong donor μ_4 sulfide and μ_2 sulfur ligands should define a common x,y plane for these coppers, with the z axis of the local g tensor of each copper oriented perpendicular to the Cu_3S_2 plane. This is

consistent with the axial nature of the g values and with the DFT calculations reported below.

Absorption and MCD The low temperature absorption and MCD spectra of a methyl viologen reduced sample of 1-hole Cu_Z are presented in Figure 3A. The absorption maximum of 1-hole Cu_Z occurs at 14,600 cm^{-1} ($\varepsilon \approx 3,000$ M^{-1} cm^{-1}), 1,000 cm^{-1} lower than the absorption maximum of 1-hole Cu_Z* (Figure 3B). There are no additional low energy intense absorption features due to the edge sulfur. The low temperature absorption and MCD spectra can be simultaneously fit to yield a total of 11 transitions, which can be assigned by considering their energies and C_o/D_o ratios, following Ref. [15] (Table S1). Comparison of the transition assignments and energies of the 1-hole Cu_Z and 1-hole Cu_Z* sites reveals some key differences. While the absorption maximum of Cu_Z occurs at lower energy than that of Cu_Z*, from MCD the three μ_4S to Cu CT transitions, assigned in Cu_Z*,[35] occur at very similar energies in the two sites (bands 5, 6, and 7, numbering given in Figure 3). The shift in the absorption maximum therefore arises from a different intensity pattern for these transitions, where in Cu_Z the lowest energy transition at 14,600 cm^{-1} is the most intense (band 5) and the transition at 15,600 cm^{-1} is weaker (band 6), but in Cu_Z* this is reversed. The μ_4S^{2-} to Cu CTs in Cu_Z* have previously been

β LUMO. Since bands 5 and 6 show the highest intensity in the 1-hole forms of Cu_Z and Cu_Z*, these must reflect charge transfer from the in-plane S $p_{x'}$ (band 6, dominant in Cu_Z* due to higher overlap with Cu_I) and S $p_{y'}$ (band 5) orbitals. Bands 6 and 5 form a pseudo-A feature in the MCD spectrum (i.e. derivative-shaped) and thus must arise from two transitions with orthogonal transition moments that spin-orbit couple in a third, mutually perpendicular direction (i.e. L_z). Since band 6 arises from a transition to Cu_I (from its dominant intensity in Cu_Z*), band 5 must reflect a transition to Cu_{IV}, since the Cu_I-S and Cu_{IV}-S bonds are close to perpendicular (96° from crystallography) while the Cu_I-S and Cu_{II}-S bonds are close to parallel (160°).[13] The change in relative intensities of the μ_4S^{2-} to Cu CT transitions in Cu_Z relative to Cu_Z*, where band 6 decreases in intensity while band 5 increases in intensity, thus indicates that there is less spin on Cu_I and more spin on Cu_{IV} in 1-hole Cu_Z relative to 1-hole Cu_Z*. This is consistent with the EPR hyperfine values, which suggest that the spin in Cu_Z is delocalized 1:1:1 over Cu_I, Cu_{II}, and Cu_{IV}, while from Ref. [35] in Cu_Z* the spin is delocalized ~5:2 over Cu_I and Cu_{IV}. Additionally, in Cu_Z*, a band at 18,000 cm^{-1} (band 8) was assigned as a high energy d-d transition due to its high C_0/D_0 ratio; this was assigned as a localized $d_{xy} \rightarrow d_{x2-y2}$ transition on Cu_I, where most of the 1-hole is localized.[35] No equivalent high energy d-d transition is observed in the MCD spectrum of Cu_Z. The lower energy of the d-d transitions in Cu_Z relative to Cu_Z* is likely due to the decreased spin on Cu_I, the only four coordinate site, relative to Cu_{II} and Cu_{IV}, which are both 3 coordinate and have a weaker ligand field.

Resonance Raman The resonance Raman spectrum of 1-hole Cu_Z and the enhancement profiles of the vibrations are presented in Figures 4A and 4B, respectively. Seven vibrations
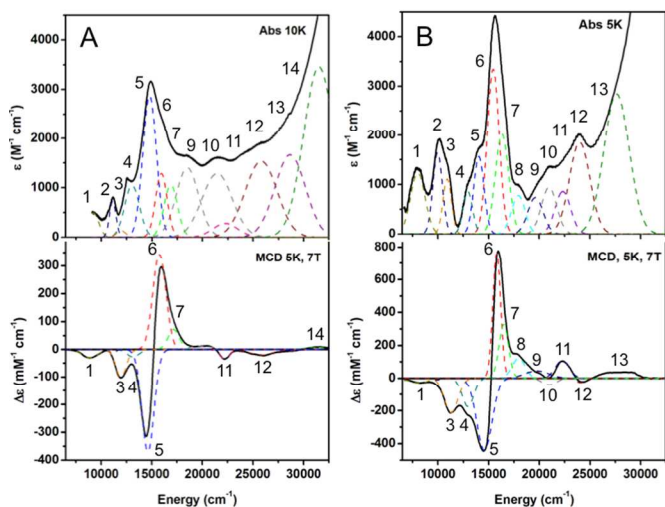

Figure 3: Low temperature absorption and MCD spectra of A) 1-hole Cu_Z, 10 K absorption, 5 K and 7 T MCD. B) 1-hole Cu_Z*, 5 K absorption, 5 K and 7 T MCD (adapted from Ref. [15]).

assigned as transitions from the three different 3p orbitals of the μ_4S^{2-} to the β LUMO of the cluster. From our current study of resting 1-hole Cu_Z* and Cu_Z with different edge ligands,[15, 35] the β LUMO is delocalized in the plane that contains Cu_I, Cu_{II}, Cu_{IV} and the μ_4S^{2-}, with different amounts of spin distributed over Cu_I, Cu_{II}, and Cu_{IV} depending on the edge ligation. Two of the μ_4S^{2-} p orbitals are in the plane, oriented between Cu_I and Cu_{IV} (S $p_{x'}$) and between Cu_{IV} and Cu_{II} (S $p_{y'}$), while the third is perpendicular to the plane (S $p_{z'}$). Scheme S1 reflects the orientation and simplified composition of these orbitals determined for 1-hole Cu_Z* from DFT calculations. The CT intensities reflect the overlap of these three S p orbitals with the
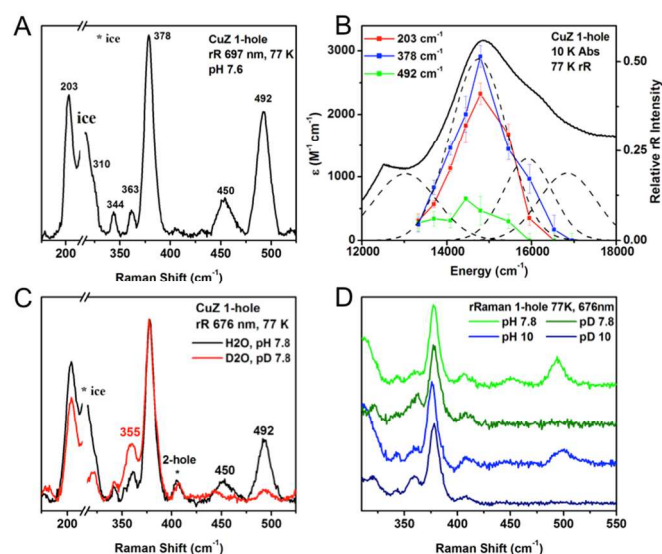

Figure 4: A) Resonance Raman spectrum of 1-hole Cu_Z at 77 K, excitation energy 697 nm. B) Excitation profile of the 203, 378, and 492 cm^{-1} vibrations. C) H-D isotope shift of the vibrations of 1-hole Cu_Z, performed in pH or pD 7.8 100 mM phosphate, excitation energy 676 nm. D) Comparison of SH bending vibrations at pH/pD 7.8 (green) and pH/pD 10 (blue).

are enhanced in the most intense S to Cu CT transition (band 5), including three intense vibrations at 203, 378, and 492 cm^{-1}. The vibration at 378 cm^{-1} occurs at the same energy as a Cu-S stretch of the Cu$_Z$* site (Figure S3) and the previously reported ^{34}S isotope sensitivities of both vibrations are similar (-5.8 and -4.7 cm^{-1}, respectively),[28] indicating that the 378 cm^{-1} vibration in 1-hole Cu$_Z$ can be assigned as a Cu-S vibration of the μ$_4$ sulfide. In contrast, the 203 cm^{-1} vibration is significantly lower in energy than the vibrations of Cu$_Z$*, and thus can be assigned as a Cu-S vibration of the μ$_2$ sulfur ligand that is only present in Cu$_Z$. Further, there are two high energy vibrations in Cu$_Z$ at 450 and 492 cm^{-1} that show significant deuterium isotope sensitivity, shifting down in energy by -137 cm^{-1} (for the 492 cm^{-1} vibration) in deuterated buffer (Figure 4C). This shift requires their assignment as S-H bending modes. Thus, we can definitively identify the edge ligand in 1-hole Cu$_Z$ as a μ$_2$SH$^-$. The S-H bending modes at 492 and 450 cm^{-1} are present at both pH 7.8 and pH 10 (Figure 4D), indicating that the pKa of the edge thiolate is ~11 or higher. This is further supported by the lack of pH dependence observed in the MCD and EPR spectra of 1-hole Cu$_Z$ between pD 6 and pD 10 (Figure S4).Since the second pKa of free hydrogen sulfide in water is 12, a pKa range of 11-12 can be estimated for the edge thiolate ligand in 1-hole Cu$_Z$.

3.2 Spectroscopy of 2-hole Cu$_Z$

Absorption The 2-hole redox state has been previously shown to be the resting redox state of Cu$_Z$. 2-hole Cu$_Z$ is diamagnetic from MCD.[19] The absorption features of 2-hole Cu$_Z$ in as-isolated N$_2$OR are present with additional spectral contributions from oxidized Cu$_A$ and some amount of 1-hole Cu$_Z$*.[26] To remove these contributions, the absorption spectrum of 2-hole Cu$_Z$ (Figure 5) was obtained after reduction with sodium
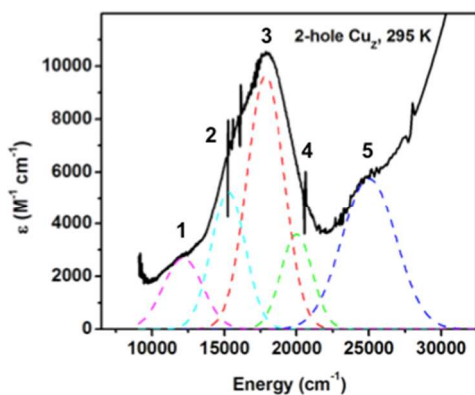

Figure 5: Absorption spectrum of 2-hole Cu$_Z$ at room temperature, obtained after ascorbate reduction of Cu$_A$ and subtraction of spectral contribution of 1-hole Cu$_Z$*.

ascorbate, which reduces the Cu$_A$ site faster than it reduces 2-hole Cu$_Z$, and subtraction of the spectral contribution of 1-hole Cu$_Z$*, obtained from a separately purified N$_2$OR sample containing 90±10% Cu$_Z$*. An intense absorption maximum for 2-hole Cu$_Z$ is observed at 18,300 cm^{-1} (ε ≈ 10,000 M^{-1} cm^{-1}) with a weaker low energy shoulder, consistent with absorption

spectra previously reported for ascorbate reduced samples containing high amounts of 2-hole Cu$_Z$.[19, 32] The low temperature absorption spectrum of 2-hole Cu$_Z$ (Figure S5) resolves this absorption maximum into three distinct absorption bands. Simulation of the room temperature absorption spectrum with transition energies derived from the low temperature spectrum distinguishes five transitions, all with absorption intensities higher than 1,000 M^{-1} cm^{-1}, sufficiently intense to be S to Cu CT transitions from the μ$_4$S^{2-} or the μ$_2$S ligand (Figure 5). The two most intense transitions (bands 2 and 3) are either from different ligands (μ$_2$S and μ$_4$S^{2-}) or from the same ligand to two different acceptor orbitals (the α and β holes of the broken symmetry singlet ground state). Based on the correlation of resonance Raman excitation profiles of the vibrations of 2-hole Cu$_Z$ to DFT calculations (vide infra), the assignment of the two transitions as CT transitions from the μ$_4$S^{2-} to two different holes is preferred.

Resonance Raman The resonance Raman spectrum of 2-hole Cu$_Z$ was obtained upon excitation into the intense absorption maximum at 18,300 cm^{-1} (Figure 6A). Two vibrations are enhanced at 350 and 405 cm^{-1}. The ^{34}S isotope shifts of these vibrations have been previously reported to be -5.6 and -5.8 cm^{-1}, respectively, indicating that they are Cu-S stretches.[28] In contrast to 1-hole Cu$_Z$, no higher energy S-H bending vibration
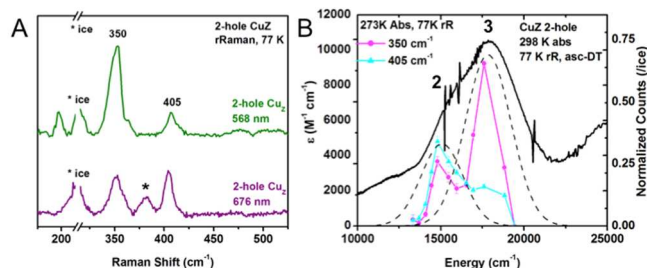

Figure 6: A) Resonance Raman spectra of 2-hole Cu$_Z$ at 77 K and two excitation energies, 568 nm (green) and 676 nm (purple). Starred vibration is due to 1-hole Cu$_Z$*. B) Excitation profiles of the 350 and 405 cm^{-1} vibrations overlaid with the room temperature absorption spectrum.

is observed (up to 800 cm^{-1}). The excitation profile of the Cu-S stretching vibrations shows that they are enhanced differently in the most intense absorption bands 2 and 3 (Figure 6B). The lower energy vibration at 350 cm^{-1} is enhanced in both transitions, while the higher energy vibration at 405 cm^{-1} is dominantly enhanced in the lower energy transition (band 2) and only weakly enhanced in band 3. This difference in profiling behavior is consistent with the Cu-S vibrations obtained computationally for a Cu$_4$S$_2$ cluster with a μ$_2$S^{2-} and μ$_4$S^{2-} and with the predicted enhancements of key vibrations in transitions from the μ$_4$S^{2-} to the α and β holes (see 3.3).

The resonance Raman spectrum 2-hole Cu$_Z$ shows no significant shift in the energies of the 350 and 405 cm^{-1} vibrations between pD 6 and pD 10 (Figure S6). This suggests that the edge ligand has a pKa either lower than 5.5 or higher than 10.5. A pKa higher than 10.5 in the 2-hole redox state is not consistent with observed pKa of 11-12 for 1-hole Cu$_Z$, as the increased charge of the 2-hole state will lead to a lower pKa

relative to the 1-hole redox state. The possibility of a pKa less than 5.5 for 2-hole Cu$_Z$ is evaluated computationally below.

3.3 Calculations

1-hole Cu$_Z$ A computational model of 1-hole Cu$_Z$ was constructed based on the crystal structure of *Pseudomonas stutzeri* N$_2$OR (PDB ID 3SBP, resolution 1.7 Å).[14] On the basis of the resonance Raman data, the edge sulfur was modeled as an SH$^-$ ligand bridging the Cu$_I$-Cu$_{IV}$ edge (Figure 7A). This will
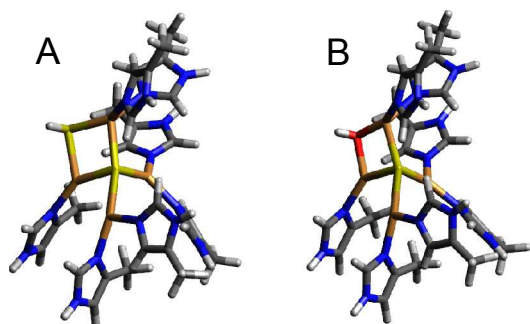

Figure 7: Computational models of A) 1-hole Cu$_Z$ and B) 1-hole Cu$_Z$* (B3LYP, TZVP on Cu, S, and ligating N atoms, and SV on all remaining atoms, PCM of 4.0).

be compared to an experimentally validated model of the Cu$_Z$* site, which has a hydroxide ligand bridging the Cu$_I$-Cu$_{IV}$ edge (Figure 7B).[15] The optimized structure of the 1-hole SH$^-$ cluster agrees well with the bond lengths and angles observed in the crystal structure (2.35 Å and 2.48 Å for the Cu$_I$-μ_2SH$^-$ and Cu$_{IV}$-μ_2SH$^-$ bonds computationally, relative to 2.61 Å and 2.49 Å crystallographically with a resolution of 1.7 Å,[14] Table S2). Since the crystal was grown from the "purple" resting form of *Ps*N$_2$OR, containing the resting 2-hole redox state of the Cu$_Z$ site, the Cu$_Z$ site in the crystal may have some photo-reduction due to exposure to X-ray radiation.[37] The calculated structures and spin distributions are not significantly perturbed when a triple zeta basis set was used on all His ring atoms (Tables S4 and S5). Including the second sphere residues Lys397 and Glu435 in the computational model also does not affect the structure or spin distribution, consistent with the small effect on the spectral features of 1-hole Cu$_Z$* observed experimentally upon deprotonation of Lys397.[15] Thus, the structures including only first sphere ligands were used to model the Cu$_Z$ and Cu$_Z$* sites in this study.

The 1-hole model with an SH$^-$ edge ligand reproduces the key spectral features observed for the 1-hole Cu$_Z$ site. The Mulliken atomic spin distribution of the cluster with an SH$^-$ edge ligand is delocalized over Cu$_I$, Cu$_{II}$, and Cu$_{IV}$ in a 2:1:1 ratio. In going from Cu$_Z$* to Cu$_Z$ the calculated spin on Cu$_I$ changes from 26% to 17% (Table 2), which is consistent with the decrease in intensity of band 6 observed in the absorption and MCD data for 1-hole Cu$_Z$ and leads to a more equal distribution of spin over Cu$_I$, Cu$_{II}$, and Cu$_{IV}$, consistent with the EPR hyperfine values. The LUMO of the Cu$_Z$ model contains d$_{x2-y2}$ character on Cu$_I$, Cu$_{II}$, and Cu$_{IV}$, which are aligned, consistent with the ground state predicted from the EPR g

Table 2: Mulliken atomic spin density of 1-hole computational models with SH$^-$ and OH$^-$ bridging ligands on the Cu$_I$-Cu$_{IV}$ edge, with % Cu and % d orbital character in their ground state wavefunctions.

Edge Ligand	Mulliken Atomic Spin Density					
	Cu$_I$	Cu$_{II}$	Cu$_{III}$	Cu$_{IV}$	μ_4S^{2-}	μ_2L$^-$
SH$^-$ bridge	0.17	0.11	0.06	0.10	0.34	0.16
OH$^-$ bridge	0.26	0.09	0.04	0.13	0.31	0.10

values (Figure S7). It also contains significant antibonding μ_4S^{2-} and μ_2SH$^-$ character, explaining why Cu-S stretching vibrations of both the μ_4S^{2-} and μ_2SH$^-$ are enhanced in the charge transfer transitions to this acceptor orbital. Additionally, the computational model predicts the Cu$_Z$ site to be more covalent than the Cu$_Z$* site, with 10% less Cu character in the ground state wavefunction, reflecting delocalization of the spin from Cu$_I$ onto the edge SH$^-$ ligand. The low g$_∥$ value for 1-hole Cu$_Z$ is also predicted by the computational model (Table S7). However, in contrast to experiment, the calculated g$_∥$ values for the Cu$_Z$ and Cu$_Z$* models differ, with a higher calculated g$_∥$ value for Cu$_Z$* than that observed experimentally. This suggests that the calculated model of Cu$_Z$* does not accurately predict the ligand field on Cu$_I$ that leads to the higher energy d$_{xy}$→d$_{x2-y2}$ transition observed experimentally.

The Cu-S stretching vibrations and S-H bending vibrations for the 1-hole SH$^-$ model of Cu$_Z$ are given in Table S8 and Figure S8. The model predicts two S-H bending modes at 426 and 461 cm^{-1} with H/D isotope shifts of -125 cm^{-1} and -123 cm^{-1}, respectively, similar to the vibrations observed experimentally at 450 and 492 cm^{-1} (with a shift of -135 cm^{-1} for the 492 cm^{-1} vibration; the 450 cm^{-1} vibration cannot be observed after deuteration due to overlap with the ice scattering peak). Equivalent O-H bends are predicted for the OH bridged Cu$_Z$* model at higher energies, but these are not experimentally observed. The Cu$_Z$ model also predicts the presence of a low energy Cu-S stretching vibration of the μ_2SH$^-$ (178 cm^{-1}, observed at 203 cm^{-1} experimentally) and both models show similar energies for the Cu-μ_4S stretching vibrations. The absolute energies of the Cu-S stretching vibrations for both the μ_4 sulfide and μ_2 thiolate are underestimated, as has been found for computational models of the Cu$_Z$* site.[15, 35] The TD DFT calculated absorption spectrum for the Cu$_Z$ model is also very similar to the calculated absorption spectrum for the Cu$_Z$* model both with B3LYP and with the functional B98, which has been shown to predict the experimental absorption spectrum of a Cu$_3$S$_2$ model complex reasonably well.[38] Interestingly, neither the experimental absorption spectrum nor the TD-DFT calculation predicts an intense low energy charge transfer transition from the μ_2SH$^-$ ligand (Figure S9). While some weak transitions predicted computationally at lower energy than the μ_4S^{2-} to Cu CT transitions have μ_2SH$^-$ to Cu CT character, they are predicted to lack intensity and are thus difficult to distinguish from the Cu d to d transitions that are also observed in this energy region.

Thus, a computational model of the tetranuclear copper cluster with an SH$^-$ edge ligand bridging Cu$_I$ and Cu$_{IV}$ provides a good structural model of 1-hole Cu$_Z$ that reproduces its key spectral features. This spectroscopically calibrated model was

then extended to the 2-hole redox state of the Cu_Z site, for which less experimental data are accessible.

2-hole Cu_Z Two possible computational models were developed for 2-hole Cu_Z, one with an edge thiolate ligand ($Cu_4S(SH)$) and one with an edge sulfide (Cu_4S_2). These were optimized in both the triplet (S=1) and broken symmetry singlet (S=0) ground spin states. For both models the singlet is lower in electronic energy, by -8.0 kcal/mol for the sulfide and -3.4 kcal/mol for the thiolate (spin corrected energies using B3LYP). The singlet state was verified to be the ground state using a variety of functionals, including M06L, M06, and TPSSh. Thus, both structures would be consistent with the experimentally determined singlet ground state of 2-hole Cu_Z.[19] The optimized structure of the 2-hole $Cu_4S(SH)$ model is similar to that of the 1-hole SH^- model of 1-hole Cu_Z, with slightly shorter Cu_I/Cu_{IV}-SH^- and Cu_I/Cu_{IV}-μ_4S bonds (Table S9). The α LUMO is dominantly localized on Cu_I and has equal μ_4S^{2-} and μ_2SH^- antibonding character (Table 3) while the β

Table 3: Mulliken spin densities on Cu and S atoms in the α and β LUMOs of the broken symmetry singlet 2-hole $Cu_4S(SH)$ and Cu_4S_2 models (B3LYP, TZVP on Cu, S, and ligating N atoms, and SV on all remaining atoms, PCM of 4.0).

		Mulliken Spin Density					
		μ_2L	Cu_I	Cu_{II}	Cu_{III}	Cu_{IV}	μ_4S^{2-}
2-hole SH^-	α LUMO	0.16	0.37	0.06	0.06	0.04	0.20
S=0	β LUMO	0.17	0.03	0.17	0.09	0.16	0.30
2-hole S^{2-}	α LUMO	0.33	0.22	0.06	0.04	0.07	0.23
S=0	β LUMO	0.37	0.05	0.06	0.05	0.14	0.27

LUMO is delocalized equally over Cu_{II} and Cu_{IV} and has more μ_4S^{2-} antibonding character. Upon deprotonation of the edge SH^-, the 2-hole Cu_4S_2 model has significantly shorter bonds between the edge sulfide and Cu_I/Cu_{IV} and similar μ_4S^{2-}-Cu bond lengths to the 2-hole SH^- model (Table S9). In this model, the α LUMO is localized on Cu_I while the β LUMO is localized on Cu_{IV} (Figure 8 and Table 3). Both holes have significant
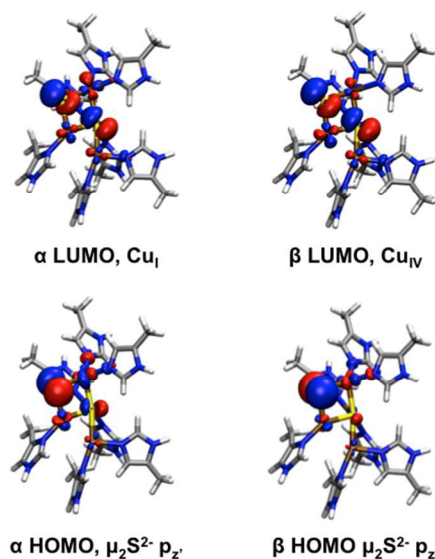

Figure 8: Frontier molecular orbitals of 2-hole Cu_Z (two sulfide model).

μ_2S^{2-} character, indicating that the edge sulfide copper bonds are highly covalent.

The energy of deprotonation calculated from the 2-hole models was compared to the calculated energy of deprotonation of the 1-hole SH^- model, where the experimentally estimated pKa of the edge thiolate is 11-12 (vide supra). Examination of the energy required to deprotonate the 1-hole and 2-hole SH^- models shows that deprotonation of the 1-hole is not energetically favored (ΔE = 26 kcal/mol, relative to an energy of -268 kcal/mol for a solvated proton)[39] while deprotonation of the 2-hole is favorable (ΔE = -9 kcal/mol). However, the two models have different charges (+2/+1 and +3/+2 for protonated and deprotonated 1-hole and 2-hole models, respectively) and this will significantly affect the relative energies of deprotonation. To minimize the charge effect, the computational models were expanded to include two second sphere Asp residues near the Cu_Z site, such that the 1-hole Cu_Z model with an edge thiolate is neutral and the 2-hole Cu_Z $Cu_4S(SH)$ model has a +1 charge. The proton transfer was performed internally to one of the Asp residues, so the total charge of the model does not change upon deprotonation (Figure S10). The $\Delta\Delta E$ for deprotonation of the 2-hole edge thiolate relative to the 1-hole species is calculated to be -25 kcal/mol (with a dielectric of 4.0). This value is dependent on the dielectric (Figure S11) and, at high dielectric values, converges to a $\Delta\Delta E$ of -12 kcal/mol. To estimate the difference in pKa between 1-hole and 2-hole Cu_Z, the $\Delta\Delta G$ was estimated from the $\Delta\Delta E$ using frequency calculations for structures with identical fixed atom constraints and thus the same number and magnitude of imaginary frequencies (these ΔG corrections vary by only 0.3 kcal/mol between the protonated and deprotonated 1-hole structures). This gives a $\Delta\Delta G$ of -12 kcal/mol for deprotonation of 2-hole versus 1-hole Cu_Z, which corresponds to a ΔpKa of -9. Given the experimental pKa value of 11-12 for the edge thiolate in 1-hole Cu_Z, these calculations predict a pKa for a thiolate in 2-hole Cu_Z of 3 or less, consistent with the absence of a pH effect in resonance Raman of 2-hole Cu_Z at pD 6. This strongly suggests that 2-hole Cu_Z is a two sulfide cluster at neutral pH.

The calculated spectral features for the Cu_4S_2 2-hole Cu_Z model can be compared with those determined experimentally. The TD DFT predicted absorption spectrum (using both B3LYP and B98) is qualitatively similar to the experimental absorption spectrum, showing two intense absorption maxima with a higher energy shoulder (Figure S12). The predicted vibrations of the 2-hole Cu_4S_2 model are given in Table S10 and Figure S13. All of the calculated vibrations are shifted up in energy in comparison to those of the 1-hole SH^- model, with the most significant energy differences observed for the sulfur edge vibrations, due to the short and highly covalent Cu-μ_2S^{2-} bonds in the 2-hole Cu_4S_2 cluster. In particular, the μ_2S^{2-}-Cu_I stretch now occurs at a similar energy to and mixes with vibrations of the μ_4S^{2-}, leading to symmetric and antisymmetric combinations of the μ_2S^{2-}-Cu_I and μ_4S^{2-}-Cu_I stretches (predicted at 312 and 309 cm^{-1}, respectively, see SI). The symmetric combination is allowed in resonance Raman and will be

enhanced in all transitions due to the high amount of μ_2S^{2-} character in both the α and β holes. This is a good candidate for the 350 cm^{-1} vibration observed experimentally that profiles in both intense absorption bands (see Figure 6B). The highest energy core vibration of the 2-hole μ_2S^{2-} cluster is a symmetric Cu_{II}-μ_4S^{2-}-Cu_{IV} stretch predicted at 344 cm^{-1} which will be selectively enhanced in a transition to the β LUMO localized on Cu_{IV} (Figure 8). A symmetric Cu_{II}-μ_4S^{2-}-Cu_{IV} stretch is also computationally predicted in the 1-hole SH$^-$ model at 320 cm^{-1} and the calculated shift in energy of this mode between the 1-hole and 2-hole models (+24 cm^{-1}) is similar to the energy increase of the highest energy Cu-S stretches observed experimentally in 1-hole and 2-hole Cu_Z (378 and 405 cm^{-1} respectively, Δv of +27 cm^{-1}). Thus, the 2-hole Cu_4S_2 model qualitatively predicts a high energy Cu-S vibration that will be selectively enhanced only in a transition to the β hole and a lower energy Cu-S vibration that will be enhanced in both intense transitions. This is consistent with the enhancement profiles of the two vibrations observed experimentally in Figure 6B. This establishes that a μ_2S^{2-} bridge is energetically favored and consistent with the spectral features of 2-hole Cu_Z.

4. Discussion

A combination of spectroscopic methods and DFT calculations has been used to define the protonation state of the μ_2 sulfur ligand on the Cu_I-Cu_{IV} edge in 1-hole and 2-hole Cu_Z. This leads to insight into the spectroscopic similarities between 1-hole Cu_Z and 1-hole Cu_Z^*, the redox reactivity of 1-hole Cu_Z in the slow 2 electron reduction of N_2O, and the interconversion between Cu_Z and Cu_Z^*, the reactive form of the cluster for N_2O reduction *in vitro*.

4.1 Protonation states of 1-hole and 2-hole Cu_Z

The protonation state of the edge ligand in 1-hole Cu_Z has been directly determined by resonance Raman spectroscopy. Two high energy vibrations are enhanced in the most intense μ_4S^{2-} to Cu CT transition of 1-hole Cu_Z, at 450 and 492 cm^{-1}, and have large isotope shifts upon solvent deuteration (-137 cm^{-1} for the 492 cm^{-1} mode). This is consistent with S-H bending modes, indicating that the μ_2S ligand is a thiolate. The energy and solvent isotope shift of these S-H bending modes are as predicted by DFT calculations for a model with a μ_2SH^- bridging the Cu_I-Cu_{IV} edge. The EPR spectrum of 1-hole Cu_Z indicates a ground state in which the spin is delocalized over 3 coppers in dominantly d_{x2-y2} orbitals. The absorption and MCD spectra show three μ_4S^{2-} to Cu charge transfer transitions that have very similar energies to those observed for 1-hole Cu_Z^* (which has a hydroxide bridged Cu_I-Cu_{IV} edge) but a different intensity pattern, consistent with a change in spin distribution in the cluster from dominantly on Cu_I in 1-hole Cu_Z^* to more evenly delocalized over Cu_I, Cu_{II}, and Cu_{IV}. This ground state spin distribution is consistent with that predicted from DFT calculations for the μ_2SH^-. Based on the absence of a pH effect in 1-hole Cu_Z up to a pH of 10, the pKa of the edge thiolate in 1-hole Cu_Z is estimated to be 11-12.

The 2-hole state of Cu_Z was also spectroscopically defined, but no direct spectroscopic evidence for the protonation state of the edge ligand was obtained. DFT calculations of the deprotonation of a μ_2SH^- ligand in 2-hole Cu_Z relative to 1-hole Cu_Z were used to determine that 2-hole Cu_Z likely has a sulfide edge ligand. Deprotonation of a μ_2SH^- ligand in the 2-hole redox state is at least 12 kcal/mol more favorable than in the 1-hole redox state, after accounting for charge and dielectric effects. This yields a calculated pKa for a μ_2SH^- ligand in 2-hole Cu_Z of 3 or less, which strongly suggests that 2-hole Cu_Z has an edge sulfide ligand at physiological pH. The calculated spectroscopic properties of a model of 2-hole Cu_Z with a μ_2S^{2-} ligand are also consistent with those observed experimentally.

4.2 Similarities between 1-hole Cu_Z and 1-hole Cu_Z^*

It has previously been observed that the spectral features of 1-hole Cu_Z are rather similar to those of 1-hole Cu_Z^*, despite the change in the nature of the edge ligand from a thiolate to a hydroxide.[19, 28] The spectroscopic similarities between 1-hole Cu_Z and 1-hole Cu_Z^* reflect similar bonding interactions between the μ_4S^{2-} and the in plane coppers (Cu_I, Cu_{II}, and Cu_{IV}) which are not significantly perturbed by the nature of edge ligand. This results in similar transition energies in the absorption and MCD spectra, as the dominant transitions are due to μ_4S^{2-} to Cu charge transfer, and a similar intense core Cu-μ_4S^{2-} stretching mode in the resonance Raman spectrum, observed at 378 cm^{-1} in both sites. Small quantitative differences in the EPR hyperfine values and transition absorption and MCD intensities between the two sites arise from a perturbation of the spin density distribution of the cluster in 1-hole Cu_Z, where the more covalent μ_2SH^- leads to delocalization of the spin on Cu_I (dominant in Cu_Z^*) onto the edge SH$^-$. Despite the higher covalency of the Cu_Z site, the g values in the EPR spectra are similar for Cu_Z and Cu_Z^*, as the localization of spin on the four coordinate Cu_I in 1-hole Cu_Z^* leads to higher energy d-d transitions, opposing the decreased covalency, leading to the net low g values also observed experimentally for Cu_Z. The difference in edge ligation in the two sites is observed primarily in the resonance Raman enhanced vibrations, where a low energy Cu-μ_2SH^- stretch at 203 cm^{-1} and higher energy S-H bending modes at 450 and 492 cm^{-1} are additionally enhanced in the dominant μ_4S^{2-} to Cu CT transition in Cu_Z but not Cu_Z^*, due to the more covalent interaction between the coppers and the edge SH$^-$. Thus, the spectral similarities between 1-hole Cu_Z and 1-hole Cu_Z^* reflect similar bonding with the μ_4S^{2-} ligand and the distribution of spin over Cu_I, Cu_{II}, and Cu_{IV}. The differences in the vibrational spectra of the two sites reflect the μ_2SH^- versus μ_2OH^- edge ligation.

4.3 Insights into reactivity of 1-hole and 2-hole Cu_Z

1-hole Cu_Z has been shown to perform a slow 2 electron reduction of N_2O under single turnover conditions, with oxidation of both 1-hole Cu_Z and reduced Cu_A to generate resting 2-hole Cu_Z and 1 electron oxidized Cu_A.[26] A structure of *Ps*N_2OR obtained from crystals pressurized with N_2O shows a

linear N$_2$O molecule binding above the Cu$_{IV}$-Cu$_{II}$ edge of the Cu$_Z$ cluster (Figure 9).[14] The O of N$_2$O is thought to be oriented
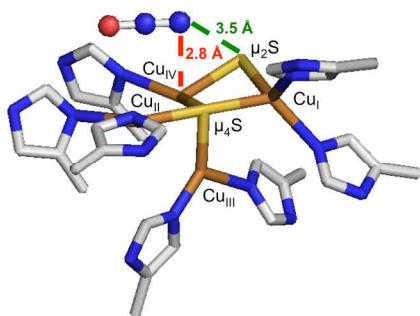

Figure 9: Crystal structure of N$_2$O bound to Cu$_Z$ (PDB ID: 3SBR, subunit C, resolution 1.7 Å).[14]

towards a solvent filled cavity between Cu$_Z$ and Cu$_A$, where there is a hydrogen bonding interaction with a localized solvent molecule, while the N end of the molecule is 2.8 Å from Cu$_{IV}$ and 3.5 Å from the μ$_2$SH$^-$ ligand. The spectroscopically and computationally defined protonation states for 1-hole and 2-hole Cu$_Z$ indicate that the 1-hole Cu$_Z$ site will donate both an electron and a proton upon oxidation, due to the significantly decreased pKa of the μ$_2$SH$^-$ in the 2-hole redox state. The participation of a proton in the reduction of N$_2$O by 1-hole Cu$_Z$ avoids the thermodynamically unfavorable 1-electron reduction of N$_2$O to N$_2$O$^-$, which is endergonic by 25.4 kcal/mol, while the proton-coupled reduction of N$_2$O to form N$_2$ and a hydroxyl radical is exergonic by 7.4 kcal/mol.[40] However, a substantial barrier exists for this process due to the fact that N$_2$O is not activated through direct interaction with Cu$_Z$ (the rate of N$_2$O reduction by 1-hole Cu$_Z$ is 2×10^{-4} s^{-1}).[26] Thus the N$_2$O may alternatively be oriented with the O atom pointed towards Cu$_Z$, where it can directly accept a proton and an electron from the μ$_2$SH$^-$ to break the N-O bond and generate resting 2-hole Cu$_Z$, with transfer of the second electron from Cu$_A$. Since no intermediate is observed in the reduction of N$_2$O by 1-hole Cu$_Z$,[26] the hydroxide product that would be formed after N-O bond cleavage would likely be rapidly protonated and released into the nearby solvent-filled cavity, rather than coordinating to the Cu$_Z$ cluster.

The 2-hole resting state of Cu$_Z$ has been defined as having a highly covalent sulfide ligand bridging the Cu$_I$-Cu$_{IV}$ edge. This resting species is potentially the starting point for the chemical conversion of Cu$_Z$ to Cu$_Z$*, the reactive form of the cluster for N$_2$O reduction.[26] In vitro, the presence of O$_2$ is thought to promote the conversion of Cu$_Z$ to Cu$_Z$*, as isolation of N$_2$OR in the presence of O$_2$ results in samples with a high proportion of resting 1-hole Cu$_Z$*, while the resting 2-hole state of Cu$_Z$ is obtained when the purification is performed in the absence of oxygen.[16] DFT calculations on the μ$_2$S^{2-} model of 2-hole Cu$_Z$ suggest that there are frontier molecular orbitals (FMOs) available to interact with O$_2$. The α and β HOMOs of 2-hole Cu$_Z$ are occupied μ$_2$S^{2-} orbitals with dominant S p$_{z'}$ character (50% and 66% μ$_2$S^{2-} respectively, Figure 8). This μ$_2$S^{2-} p$_{z'}$ orbital is oriented perpendicular to the Cu$_3$S$_2$ plane, towards the

solvent-filled cavity where N$_2$O, and by analogy O$_2$, would access the Cu$_Z$ cluster. Based on these FMOs, reaction of the Cu$_Z$ site with O$_2$ would proceed via oxidation of the edge sulfide, rather than by a Cu-based oxidation. Since this is a four electron process, there will in principle also be electrons available from the sulfide for the reduction of the copper site, dependent on the nature of the oxidized sulfur product. However, it is unlikely that this is the mechanism involved in interconversion of Cu$_Z$ and Cu$_Z$* in vivo, since resting Cu$_Z$* has been isolated under exclusion of oxygen conditions from anaerobically grown cells in bacterial strains with accessory genes knocked-out.[41] Thus, the in vivo mechanism for interconversion of Cu$_Z$ and Cu$_Z$*, which is required to maintain N$_2$OR in the reactive Cu$_Z$* form, and the role of accessory proteins in this process, remain to be identified.

5. Conclusions

We have used a combination of spectroscopies and DFT calculations to determine the protonation states of the edge sulfur in the 1-hole and 2-hole redox states of Cu$_Z$. From resonance Raman spectroscopy, 1-hole Cu$_Z$ has a μ$_2$ thiolate ligand with a pKa of 11-12, due to the presence of S-H bending modes that are not perturbed up to pH 10. DFT calculations of a 1-hole cluster with a μ$_2$SH$^-$ ligand reproduce the key spectral features of 1-hole Cu$_Z$. The computational modeling of the 2-hole Cu$_Z$ site indicates that the edge ligand is a μ$_2$S^{2-} with a pKa of 3 or less, which is consistent with the absorption and resonance Raman features of 2-hole Cu$_Z$. The nature of this edge ligand has been used to obtain insight into the slow reduction of N$_2$O by 1-hole Cu$_Z$ and suggest how 2-hole Cu$_Z$ might react with O$_2$, a possible route for the conversion of Cu$_Z$ to Cu$_Z$* in vitro.

6. Acknowledgements

Notes and references

^{a} Department of Chemistry, Stanford University, Stanford, CA 94305
^{b} Dipartimento di Chimica, Università di Pavia, Via Taramelli 12, 27100 Pavia, Italy
^{c} UCIBIO, REQUIMTE, Departamento de Química, Faculdade de Ciências e Tecnologia, Universidade Nova de Lisboa, 2829-516 Caparica, Portugal

Electronic Supplementary Information (ESI) available: Full experimental and computational methodology, EPR quantification of the Cu$_Z$*/Cu$_Z$

ratio, 2nd derivative of the X band EPR of 1-hole Cu$_Z$, table of absorption band energies and assignments for 1-hole Cu$_Z$ and 1-hole Cu$_Z$*, resonance Raman spectrum and profile of 1-hole Cu$_Z$*, pH dependence of the spectral features of 1-hole and 2-hole Cu$_Z$, low temperature absorption spectrum of 2-hole Cu$_Z$, and computational structures, vibrations, and TD-DFT absorption spectra for models of 1-hole and 2-hole Cu$_Z$ (1-hole SH$^-$ and OH$^-$ and 2-hole SH$^-$ and S^{2-} models). See DOI: 10.1039/b000000x/

1. P. Tavares, A. S. Pereira, J. J. G. Moura and I. Moura, *Journal of Inorganic Biochemistry*, 2006, **100**, 2087-2100.

2. A. J. Thomson, G. Giannopoulos, J. Pretty, E. M. Baggs and D. J. Richardson, *Philosophical Transactions of the Royal Society B-Biological Sciences*, 2012, **367**, 1157-1168.

3. W. G. Zumft and P. M. H. Kroneck, *Advances in Microbial Physiology*, 2007, **52**, 107-227.

4. B. Bates, Z. W. Kundzewicz, S. Wu, N. Arnell, V. Burkett, P. Döll, D. Gwary, C. Hanson, B. Heij, B. Jiménez, G. Kaser, A. Kitoh, S. Kovats, P. Kumar, C. Magadza, D. Martino, L. J. Mata, M. Medany, K. Miller, T. Oki, B. Osman, J. Palutikof, T. Prowse, R. Pulwarty, J. Räisänen, J. Renwick, F. Tubiello, R. Wood, Z.-C. Zhao, J. Arblaster, R. Betts, A. Dai, C. Milly, L. Mortsch, L. Nurse, R. Payne, I. Pinskwar and T. Wilbanks, ed. I. Secretariat, 2008.

5. D. Richardson, H. Felgate, N. Watmough, A. Thomson and E. Baggs, *Trends in Biotechnology*, 2009, **27**, 388-397.

6. A. R. Ravishankara, J. S. Daniel and R. W. Portmann, *Science*, 2009, **326**, 123-125.

7. K. Butterbach-Bahl, E. M. Baggs, M. Dannenmann, R. Kiese and S. Zechmeister-Boltenstern, *Philosophical Transactions of the Royal Society B-Biological Sciences*, 2013, **368**.

8. L. Bergaust, Y. J. Mao, L. R. Bakken and A. Frostegard, *Applied and Environmental Microbiology*, 2010, **76**, 8285-8285.

9. L. R. Bakken, L. Bergaust, B. B. Liu and A. Frostegard, *Philosophical Transactions of the Royal Society B-Biological Sciences*, 2012, **367**, 1226-1234.

10. S. Saleh-Lakha, K. E. Shannon, S. L. Henderson, B. J. Zebarth, D. L. Burton, C. Goyer and J. T. Trevors, *Applied and Environmental Microbiology*, 2009, **75**, 5082-5087.

11. J. Sorensen, J. M. Tiedje and R. B. Firestone, *Applied and Environmental Microbiology*, 1980, **39**, 105-108.

12. N. Morley and E. M. Baggs, *Soil Biology & Biochemistry*, 2010, **42**, 1864-1871.

13. K. Brown, K. Djinovic-Carugo, T. Haltia, I. Cabrito, M. Saraste, J. J. G. Moura, I. Moura, M. Tegoni and C. Cambillau, *Journal of Biological Chemistry*, 2000, **275**, 41133-41136.

14. A. Pomowski, W. G. Zumft, P. M. H. Kroneck and O. Einsle, *Nature*, 2011, **477**, 234-U143.

15. S. Ghosh, S. I. Gorelsky, S. D. George, J. M. Chan, I. Cabrito, D. M. Dooley, J. J. G. Moura, I. Moura and E. I. Solomon, *Journal of the American Chemical Society*, 2007, **129**, 3955-3965.

16. W. G. Zumft, C. L. Coyle and K. Frunzke, *Febs Letters*, 1985, **183**, 240-244.

17. S. Dell'Acqua, S. R. Pauleta, J. J. G. Moura and I. Moura, *Philosophical Transactions of the Royal Society B-Biological Sciences*, 2012, **367**, 1204-1212.

18. M. Prudencio, A. S. Pereira, P. Tavares, S. Besson, I. Cabrito, K. Brown, B. Samyn, B. Devreese, J. Van Beeumen, F. Rusnak, G. Fauque, J. J. G. Moura, M. Tegoni, C. Cambillau and I. Moura, *Biochemistry*, 2000, **39**, 3899-3907.

19. T. Rasmussen, B. C. Berks, J. N. Butt and A. J. Thomson, *Biochemical Journal*, 2002, **364**, 807-815.

20. E. I. Solomon, D. E. Heppner, E. M. Johnston, J. W. Ginsbach, J. Cirera, M. Qayyum, M. T. Kieber-Emmons, C. H. Kjaergaard, R. G. Hadt and L. Tian, *Chemical Reviews*, 2014, **114**, 3659-3853.

21. A. Wuest, L. Schneider, A. Pomowski, W. G. Zumft, P. M. H. Kroneck and O. Einsle, *Biological Chemistry*, 2012, **393**, 1067-1077.

22. S. R. Pauleta, S. Dell'Acqua and I. Moura, *Coordination Chemistry Reviews*, 2013, **257**, 332-349.

23. C. L. Coyle, W. G. Zumft, P. M. H. Kroneck, H. Korner and W. Jakob, *European Journal of Biochemistry*, 1985, **153**, 459-467.

24. S. Ghosh, S. I. Gorelsky, P. Chen, I. Cabrito, J. J. G. Moura, I. Moura and E. I. Solomon, *Journal of the American Chemical Society*, 2003, **125**, 15708-15709.

25. J. M. Chan, J. A. Bollinger, C. L. Grewell and D. M. Dooley, *Journal of the American Chemical Society*, 2004, **126**, 3030-3031.

26. E. M. Johnston, S. Dell'Acqua, S. Ramos, S. R. Pauleta, I. Moura and E. I. Solomon, *Journal of the American Chemical Society*, 2014, **136**, 614-617.

27. T. Rasmussen, B. C. Berks, J. Sanders-Loehr, D. M. Dooley, W. G. Zumft and A. J. Thomson, *Biochemistry*, 2000, **39**, 12753-12756.

28. M. L. Alvarez, J. Y. Ai, W. Zumft, J. Sanders-Loehr and D. M. Dooley, *Journal of the American Chemical Society*, 2001, **123**, 576-587.

29. V. S. Oganesyan, T. Rasmussen, S. Fairhurst and A. J. Thomson, *Dalton Transactions*, 2004, 996-1002.

30. T. Rasmussen, B. C. Berks and A. J. Thomson, *Journal of Inorganic Biochemistry*, 2001, **86**, 393-393.

31. J. A. Farrar, A. J. Thomson, M. R. Cheesman, D. M. Dooley and W. G. Zumft, *Febs Letters*, 1991, **294**, 11-15.

32. J. A. Farrar, W. G. Zumft and A. J. Thomson, *Proceedings of the National Academy of Sciences of the United States of America*, 1998, **95**, 9891-9896.

33. W. E. Antholine, P. M. H. Kroneck and W. G. Zumft, *Molecular Physics*, 1998, **95**, 1247-1253.

34. M. J. Frisch, G. W. Trucks, H. B. Schlegel, G. E. Scuseria, M. A. Robb, J. R. Cheeseman, G. Scalmani, V. Barone, B. Mennucci, G. A. Petersson, H. Nakatsuji, M. Caricato, X. Li, H. P. Hratchian, A. F. Izmaylov, J. Bloino, G. Zheng, J. L. Sonnenberg, M. Hada, M. Ehara, K. Toyota, R. Fukuda, J. Hasegawa, M. Ishida, T. Nakajima, Y. Honda, O. Kitao, H. Nakai, T. Vreven, J. A. Montgomery Jr., J. E. Peralta, F. Ogliaro, M. J. Bearpark, J. Heyd, E. N. Brothers, K. N. Kudin, V. N. Staroverov, R. Kobayashi, J. Normand, K. Raghavachari, A. P. Rendell, J. C. Burant, S. S. Iyengar, J. Tomasi, M. Cossi, N. Rega, N. J. Millam, M. Klene, J. E. Knox, J. B. Cross, V. Bakken, C. Adamo, J. Jaramillo, R. Gomperts, R. E. Stratmann, O. Yazyev, A. J. Austin, R. Cammi, C. Pomelli, J. W. Ochterski, R. L. Martin, K. Morokuma, V. G. Zakrzewski,

G. A. Voth, P. Salvador, J. J. Dannenberg, S. Dapprich, A. D. Daniels, Ö. Farkas, J. B. Foresman, J. V. Ortiz, J. Cioslowski and D. J. Fox, Gaussian, Inc., Wallingford, CT, USA, 2009.

35. P. Chen, I. Cabrito, J. J. G. Moura, I. Moura and E. I. Solomon, *Journal of the American Chemical Society*, 2002, **124**, 10497-10507.

36. P. Chen, S. D. George, I. Cabrito, W. E. Antholine, J. J. G. Moura, I. Moura, B. Hedman, K. O. Hodgson and E. I. Solomon, *Journal of the American Chemical Society*, 2002, **124**, 744-745.

37. A. Pomowski, W. G. Zumft, P. M. H. Kroneck and O. Einsle, *Acta Crystallographica Section F-Structural Biology and Crystallization Communications*, 2010, **66**, 1541-1543.

38. I. Bar-Nahum, A. K. Gupta, S. M. Huber, M. Z. Ertem, C. J. Cramer and W. B. Tolman, *Journal of the American Chemical Society*, 2009, **131**, 2812-+.

39. R. M. Noyes, *Journal of the American Chemical Society*, 1962, **84**, 513-&.

40. W. H. Koppenol, *Free Radical Biology and Medicine*, 1991, **10**, 85-87.

41. P. Wunsch, H. Korner, F. Neese, R. J. M. van Spanning, P. M. H. Kroneck and W. G. Zumft, *Febs Letters*, 2005, **579**, 4605-4609.

Chemical Science Accepted Manuscript